Road Surface Roughness Estimation Using Spaceborne Synthetic Aperture Radar

Arun Babu, *Graduate Student Member, IEEE*, Dominik Gerber, Stefan V. Baumgartner, *Senior Member, IEEE*, and Gerhard Krieger, *Fellow, IEEE*

Abstract—**Road surface roughness is a major factor that is responsible for the skid resistance of vehicles and, thus, road safety. Therefore, it needs to be monitored regularly to ensure that the roughness values are in the optimal range and to perform maintenance actions when needed. Synthetic aperture radar (SAR) backscatter is sensitive to surface roughness and can provide large-scale estimates of road surface roughness. In this letter, a semi-empirical model for estimating road surface roughness using high-resolution spaceborne X-band SAR datasets from Germany's TerraSAR-X satellite is proposed for the first time. The method is capable of handling the low signal-to-noise ratio (SNR) of spaceborne SAR. To enhance the reliability of the results obtained from rather low SNR datasets, techniques such as SNR thresholding, multi-dataset fusion, and automatic road extraction were implemented. The study's results show good agreement with ground truth data.**

Index Terms—**Synthetic aperture radar, spaceborne radar, surface roughness, vehicle safety, signal-to-noise ratio.**

I. INTRODUCTION

THE road infrastructure is crucial for a country's development since it facilitates the movement of people and goods. The safety of people and vehicles using roads is also influenced by the quality of the road surface. Road surface roughness plays a significant role in road safety and quality [1]. The amount of friction between the road and the tires of vehicles is determined by the material and roughness of the road surface, which affects the grip and skid resistance of vehicles, influencing their acceleration, maneuverability, and braking performance [2]. To maintain the safety and quality of road surfaces, regular inspections are necessary to ensure that surface roughness values fall within acceptable limits [3].

Currently, measuring road friction involves driving survey vehicles with measuring devices over highways and important roads, which is time and personnel-consuming, and costly. As a result, this survey is usually conducted every few years, such as in Germany, where it occurs around every 4 years [4]. However, road wear happens annually, particularly during winter due to repeated freeze-thaw cycles [5]. Thus, more frequent monitoring of road surfaces is required.

SAR remote sensing is suitable for estimating wide-area road surface roughness because the backscattered signal received by the SAR system is sensitive to the surface's dielectric constant and roughness. In [3], high-resolution fully polarimetric airborne X-band SAR data acquired by the F-SAR sensor of the German Aerospace Center (DLR) were used to generate accurate road surface roughness images. Airborne SAR-based road monitoring, though effective, is constrained by the need for flight planning, high operational costs, and limited coverage. This can be addressed by high-resolution spaceborne SAR, which can efficiently perform repeated data acquisition of any area at a lower cost.

This letter assesses the potential of high-resolution X-band spaceborne SAR data from the TerraSAR-X (TS-X) satellite for road roughness estimation. The semi-empirical road surface roughness estimation model developed for F-SAR, which is based on the assumptions from the Dubois model [6], is used as a basis [3]. Compared to F-SAR, TS-X datasets are generally single-polarized and have lower SNR and worse resolution. Thus, this study adapted the semi-empirical model and processing chain developed for F-SAR to estimate road surface roughness using TS-X datasets. The model and processing chain have been adapted to handle single-polarized TS-X data, and they utilize SNR improvement techniques such as multilooking. Additionally, the processing chain includes techniques such as high backscatter and low SNR thresholding to eliminate highly reflective and unreliable pixels from the final surface roughness images. To enhance the robustness of the processing chain, the fusion of multiple datasets and automatic generation of surface roughness images for roads of interest were added. The credibility of the results was also tested with reference data.

II. TEST SITES

Two test sites were chosen to represent road surfaces with varying materials and roughness values. The first site is the Kaufbeuren airfield in Bavaria, Germany, including asphalt and concrete surfaces like runways, taxiways, and parking areas. Due to its inactive status, the airfield lacks regular maintenance, resulting in the presence of rough and cracked surfaces. Ground truth (GT) measurements of surface roughness were taken from multiple locations on the runway and parking area, encompassing various surface types and material compositions. Additionally, surface roughness images derived from airborne X-band F-SAR datasets are available for this test site, facilitating comparisons. Further details about this test site and

GT data collection activity can be found in [3].

The second test site is the A2-A391 motorway crossing in Braunschweig, Germany, consisting of highways, flyovers, and bridges. While a relatively uniform surface roughness is expected, variations are anticipated at bridge locations due to different construction materials (cf. Fig. 7).

III. DATASETS

In this section, the details about the spaceborne SAR datasets and ground truth data used in this study are discussed.

A. Spaceborne SAR datasets

The TS-X satellite has multiple imaging modes: staring spotlight (ST), high-resolution spotlight (HS), stripmap (SM), and ScanSAR (SC). These modes provide approximate spatial resolutions (azimuth x range) of 0.24 x 0.60 m (ST), 1.1 x 1.2 m (HS), 3.3 x 1.2 m (SM), and 18.5 x 1.2 m (SC). The swath coverage (azimuth x range) for each mode is 3.7 x 4 km (ST), 5 x 10 km (HS), 50 x 30 km (SM), and 150 x 100 km (SC) [7].
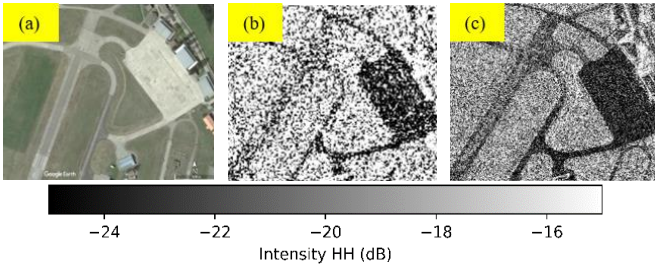

Fig. 1. Comparison of TS-X imaging modes. (a) GE image of the Kaufbeuren runway. Intensity images in (b) SM, and (c) ST modes.

TABLE I
METADATA OF THE ST MODE TS-X DATASETS

Test site	Date	Pol	Incidence angle (°)	Use
Kaufbeuren	16.03.2014	HH	43.7	Train
Braunschweig	30.04.2015	HH	39.3	Test
Kaufbeuren	13.08.2022	VV	31.6	Train
Kaufbeuren	23.09.2022	VV	43.7	Train
Kaufbeuren	29.09.2022	VV	31.0	Test

Fig. 1(a) presents the Google Earth (GE) image of a section of the Kaufbeuren runway, while Figs. 1(b) and (c) display TS-X HH polarized intensity images of the same section captured in SM and ST modes, respectively. The images have a scene center incidence angle of approximately 44 degrees. Since a dataset with a similar incidence angle range is unavailable, the HS mode image is not included in this comparison. Only the ST mode image owing to its highest spatial resolution shows clearly the reflectivity changes on the runway, which is evident when comparing it with the GE image. Hence, only ST-mode datasets are used in this study and their metadata are given in Table I.

B. Ground truth data

To train the semi-empirical surface roughness estimation model and validate the roughness values estimated using the TS-X datasets, GT surface roughness values were measured from the Kaufbeuren test site. Eight 1 m² areas on the Kaufbeuren runway and taxiway were selected as GT spots [3]. The vertical

surface undulation of the asphalt/concrete surface was measured using a handheld laser scanner with micrometer accuracy. Since Root Mean Squared (RMS) height (h_{rms}) is a commonly used metric to measure surface roughness, the height values obtained from the laser scanner measurements were used to compute a single ground truth surface roughness value ($GT\ h_{rms}$) for each location. The RMS height was computed using the formula shown below (1) [8], [9]:

$$h_{rms} = \sqrt{\frac{\sum_{i=1}^{n}(h_i - \overline{h})^2}{n-1}} \tag{1}$$

where n represents the number of samples within a 1 m² area, h_i is the height of the ith sample and $\overline{h}$ is the mean height over all samples.

IV. METHODOLOGY

This section explains the methodology for estimating road surface roughness using TS-X datasets. The flowchart of the complete processing chain is shown in Fig. 2.

A. Radiometric calibration and multilooking

The TS-X dataset is radiometrically calibrated to produce the sigma nought (σ^o) backscatter image. The σ^o values are estimated for each pixel without any spatial averaging, and the noise-equivalent beta nought (NEBN) values are estimated and subtracted from the σ^o values to minimize additive noise [10]. This noise-minimized σ^o image facilitates comparison of backscatter measurements between surfaces and enables estimation of surface properties such as roughness. Subsequently, multilooking is applied in the spatial domain to reduce speckle and enhance the SNR by averaging neighboring pixels in both range and azimuth directions [11]. The sliding window size for the spatial averaging is determined based on the smallest multilooking factors necessary in azimuth and range directions to create approximately square pixels, facilitating easier image interpretation (e.g., a 5x1 window (azimuth x range) for the ST mode dataset with a 43.7 degrees incidence angle). The σ^o image and the local incidence angle values (θ) are used as input to the surface roughness estimation model.

B. Adaptation of the road surface roughness estimation model

In the previous section, it was shown that h_{rms} is used as the measure of road roughness. However, h_{rms} cannot be estimated from the SAR data. Instead, the effective vertical surface roughness parameter (ks) can be estimated from the SAR data and it can then be inverted to estimate h_{rms} as shown below (2) [3], [8]:

$$h_{rms} = \frac{ks}{(2\pi/\lambda_c)} \tag{2}$$

where λ_c is the wavelength of the SAR system.

The mathematical formulation of the semi-empirical road surface roughness estimation model developed at DLR for the airborne SAR case is given as (3):

$$ks = 10^{\left[\frac{\log(\sigma_{pq}^o) - \log(\delta(\cos(\theta))^\beta)}{\varepsilon \sin(\theta)}\right]}. \tag{3}$$

where ks is the effective vertical surface roughness, σ_{pq}^o is the σ^o value for the p transmitted and q received polarization and
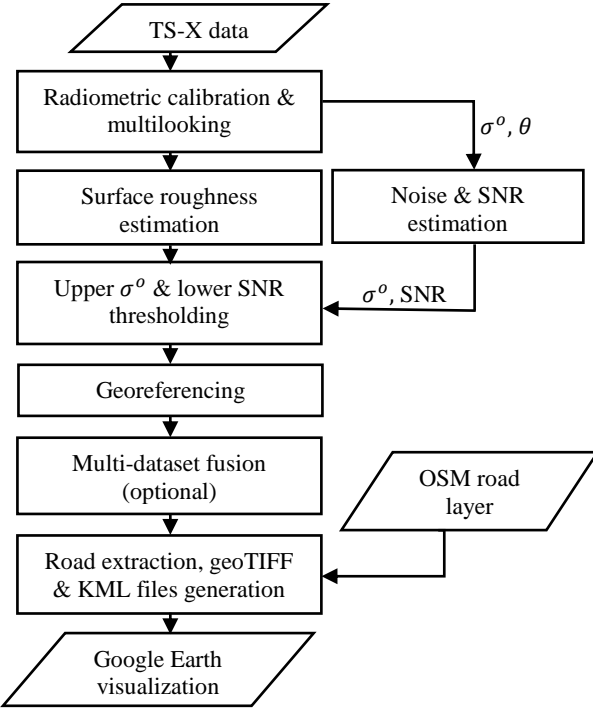
Fig. 2. Flowchart showing the complete processing chain.

θ is the local incidence angle. δ, β, and ε are the model coefficients. This model has a validity range of $ks < 2.5$ and for $\theta > 30^o$. For the X-band SAR used in this study, this translates to an h_{rms} validity range of $h_{rms} < 12.43$ mm. More details on the development of this model can be found in [3].

TABLE II
COEFFICIENTS OF THE ROUGHNESS ESTIMATION MODEL FOR TS-X DATASETS

Coefficients	Polarization	
	HH	VV
δ	0.16373946	0.17887929
β	-0.10682052	-3.95021343
ε	1.99490104	3.38223192

To make this model suitable for TS-X data, it's necessary to estimate a new set of δ, β, and ε coefficients that are specific to the TS-X datasets. It's worth noting that the TS-X ST mode datasets used in this study have different characteristics than the F-SAR datasets since they are single-polarized with a coarser resolution. To estimate the new coefficients, a least square-based curve fitting algorithm is used to train the model using the GT h_{rms}, σ_{pq}^o, and θ values at the GT spots from the TS-X datasets selected for model training (see Table I). Due to the limited availability of GT spots (only eight), the h_{rms} values estimated using the F-SAR datasets from selected locations on the Kaufbeuren runway were used as additional GT values for estimating the model coefficients. Table II shows the model coefficients estimated for the TS-X data. The coefficients are estimated separately for the HH and VV polarized datasets.

C. Upper sigma nought and lower SNR thresholding

High backscattering from objects such as lane dividers, flyover/bridge walls, overhead signboards, etc., can cause very high σ^o values from the road surface. This may result in incorrect and invalid surface roughness (h_{rms}) estimation in

these regions. To remove these values from the h_{rms} image, an upper σ^o thresholding approach is utilized. In this study, all h_{rms} image pixels with a σ^o value above -10 dB are considered invalid for the analyzed TS-X datasets. This is because the highest observed σ^o value on the road surfaces is just below -10 dB in the TS-X datasets.
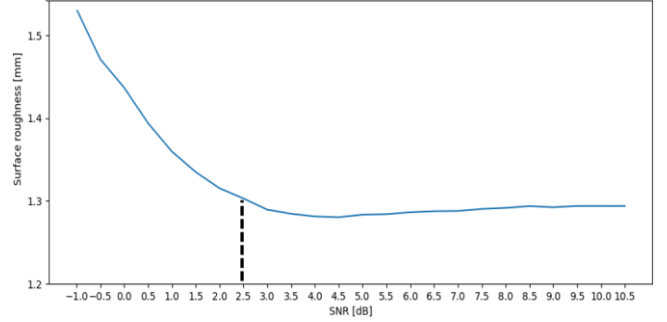

Fig. 3. Surface roughness vs. SNR plot for lower SNR threshold estimation

Low SNR pixels can also cause incorrect estimates of h_{rms}, since they contain more noise than the actual backscattered signal. Therefore, these noisy pixels must be removed from the h_{rms} image by applying an SNR threshold. To determine this threshold, a high SNR area on the Kaufbeuren runway was selected, and random Gaussian noise was gradually added to the data until the SNR reached a lower value of 2.5 dB. Below this value, a significant increase in h_{rms} was observed (cf. Fig. 3). Therefore, all pixels with an SNR below 2.5 dB were masked out from the h_{rms} image.

D. Multi-dataset fusion

The h_{rms} image obtained from a TS-X dataset with a specific acquisition geometry can have unreliable h_{rms} values due to various factors such as a very shallow incidence angle, speckle, and very low SNR regions. These errors can be minimized by fusing h_{rms} images obtained from multiple TS-X datasets with different incidence angles and acquisition geometries to create a single h_{rms} image.

Two fusion methods were implemented in this study. Before fusion, both methods exclude pixels with invalid h_{rms} values using upper σ^o and lower SNR thresholds for reliability. The first, highest SNR method, relies on h_{rms} values from the TS-X datasets with the highest SNR, as noise in the radar signal, is the least. It involves a pixel-wise SNR search across datasets. The final h_{rms} image comes solely from the highest SNR pixels in all datasets. This enhances fine road details but is sensitive to local backscatter variations from oriented features. The second method, multi-dataset averaging, treats all TS-X-derived h_{rms} values as reliable. It generates the final h_{rms} image by averaging h_{rms} values from all datasets, resulting in a smoother image that may lose some small road details [3].

E. Road extraction and Google Earth visualization

The h_{rms} image provides roughness information for the entire area, including roads, fields, houses, and forests. However, it is important to note that the roughness model is exclusively trained for estimating the millimeter scale roughness values that can be expected on road surfaces. As a result, h_{rms} values beyond the road surfaces may fall outside the model's validity range and may not be trustworthy. Moreover, for end-users, it

is more relevant to see only the roughness information of the roads. To achieve this, Open Street Map (OSM) road layers are used to create a mask for the roads of interest within the TS-X dataset extent. Finally, KML files are generated to visualize the h_{rms} images on Google Earth. Furthermore, a geoTIFF image is also provided.

V. EXPERIMENTAL RESULTS AND DISCUSSION

The experimental results obtained using the methods described in the previous section are discussed here.

Fig. 4 shows SNR plots created for the Kaufbeuren runway, indicating the SNR at 40 arbitrarily selected locations from one end of the runway to the other for datasets with different incidence angles and polarizations. Fig. 4 indicates that the concrete surface has a higher SNR compared to the asphalt surface, implying that it is rougher and reflects more signals to the radar. The HH polarization dataset, especially in asphalt areas, has the lowest SNR, making it unsuitable for accurate roughness estimation. However, the VV polarization data display higher SNR, with the VV dataset at 31.6^o having the highest SNR among them. Hence, TS-X VV polarization datasets at 30-35 degrees incidence angles are ideal for road surface roughness estimation, ensuring the minimum required SNR of 2.5 dB (cf. Fig. 3) in both concrete and asphalt regions. This also aligns with the roughness estimation model's validity range, starting from 30 degrees onward.

Fig. 5 presents h_{rms} images of a section of the Kaufbeuren runway. After road extraction and KML file creation, the images were overlaid on GE. In Fig. 5(a), the GE image shows the runway with areas of asphalt, smooth concrete, and rough concrete with repeated cuts. The h_{rms} image in Fig. 5(b) is estimated using the F-SAR dataset (resolution: approximately 25 x 25 cm). Comparing Fig. 5(b) with Fig. 5(a), asphalt areas appear blue indicating low h_{rms} values, while smooth concrete areas appear rougher and are indicated by cyan. Concrete areas with repeated cuts exhibit the highest roughness level, represented by yellow. Fig. 5(c) displays the h_{rms} image generated using the TS-X HH polarization dataset. Most pixels from asphalt and smooth concrete areas are masked out due to an SNR lower than the 2.5 dB threshold. In Fig. 5(d), the h_{rms} image is estimated using the TS-X VV polarization dataset. Fig. 5(d) has more valid pixels compared to Fig. 5(c) due to the higher SNR provided by the VV polarization dataset. Asphalt areas are indicated by blue, while smooth concrete areas appear rougher in cyan. The concrete areas with cuts have the highest roughness level, represented by yellow with a value of approximately 2.25 mm. These findings align with the h_{rms} results from the F-SAR dataset in Fig. 5(b). Fig. 5(e) and (f) show the h_{rms} images obtained by fusing multiple datasets using the highest SNR method and the multi-dataset averaging method, respectively. The fusion involves all three VV-polarized TS-X datasets listed in Table I. In both images, asphalt areas are represented in blue to cyan colors, and smooth concrete areas appear entirely in cyan. Fig. 5(e) exhibits more yellow pixels in the concrete area with cuts compared to Fig. 5(f), indicating a higher level of surface roughness. In both cases, the results closely agree with the F-SAR results.

Fig. 6 shows the comparison of h_{rms} plots from TS-X and F-SAR datasets with GT h_{rms} plot. The black plot shows the
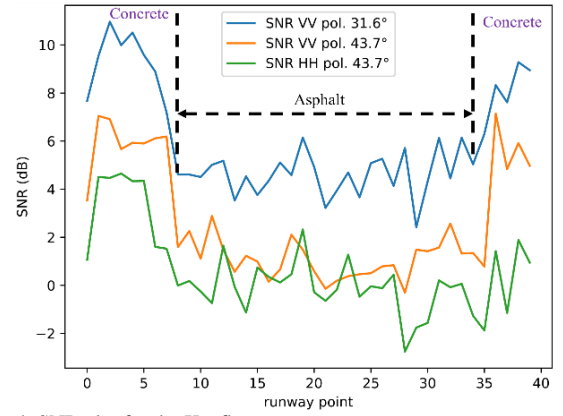

Fig. 4. SNR plot for the Kaufbeuren runway

GT h_{rms} values for the eight GT spots, while the blue plot shows the estimated h_{rms} values for the GT spots from the F-SAR dataset. Although the blue plot correlates with the GT h_{rms} plot, over- and underestimations are evident for some GT spots. Overall, the plots have an RMSE of 0.30 mm. The green plot represents h_{rms} values estimated using the VV-polarized TS-X dataset with an incidence angle of 31.6^o, which closely matches the GT h_{rms} plot with an RMSE of 0.32 mm. It should be noted that this dataset was used to estimate the model coefficients and the F-SAR h_{rms} data with an RMSE of 0.30 mm was used as additional reference data. Therefore, the RMSE of the TS-X roughness data cannot be smaller than 0.30 mm. The orange plot generated by the multi-dataset fusion using the highest SNR method overestimates the h_{rms} values and gives the highest RMSE of 0.51 mm, which is probably due
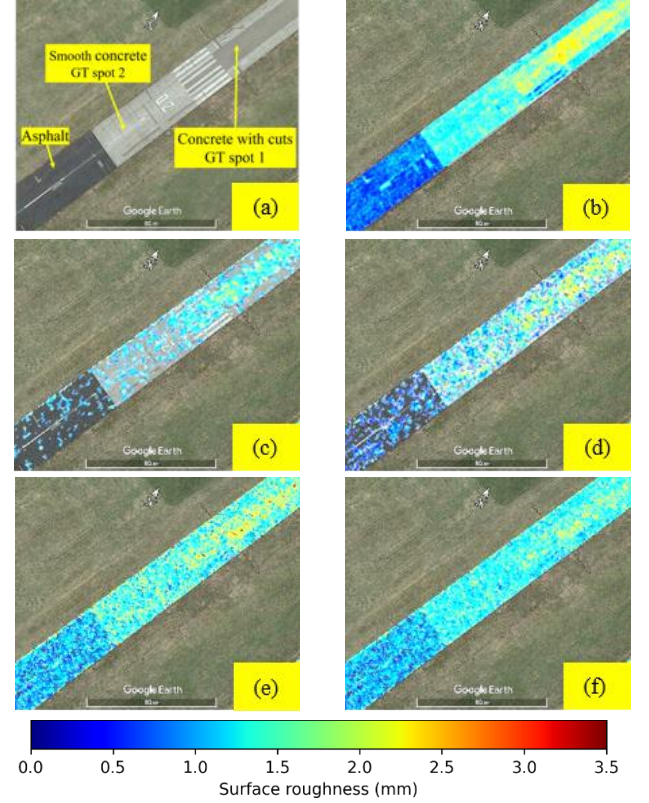

Fig. 5. Images of the Kaufbeuren runway. (a) GE image. h_{rms} images from (b) F-SAR, (c) TS-X HH pol, (d) TS-X VV pol, multi-dataset fusion using (e) highest SNR method and using (f) multi-dataset averaging method.
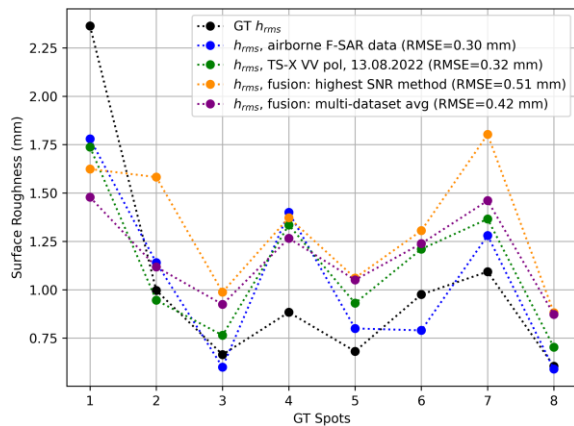
Fig. 6. Comparison of h_{rms} plots from TS-X and F-SAR datasets with GT h_{rms} plot
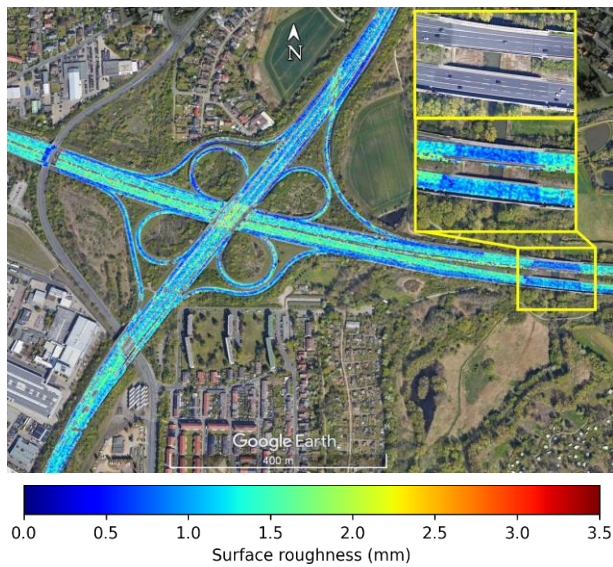

Fig. 7. h_{rms} image from TS-X HH polarized dataset for Braunschweig test site (A2-A391 motorway crossing).

to the sensitivity to local backscatter variations. The purple plot, produced by the multi-dataset averaging fusion method, has an RMSE of 0.42 mm with the GT h_{rms} plot. It should be noted here that the dotted lines connect the h_{rms} values between the GT spots, which facilitates the comparison of variability and trends between the estimated h_{rms} and GT h_{rms} values without implying a continuous relationship between the GT spots. In short, Fig. 6 indicates that the TS-X VV polarized datasets can reliably estimate the h_{rms} values with a comparable RMSE to the F-SAR and GT data.

The h_{rms} image for the Braunschweig test site generated using the TS-X HH polarized dataset is shown in Fig. 7. Due to the unavailability of VV polarized datasets, a HH polarized dataset was used for this example. The lower SNR thresholding was not applied to this image due to the low SNR of the HH polarized dataset for roads. As a result, the absolute values of h_{rms} are less accurate. However, qualitative comparisons of h_{rms} values can still be made. The south-north highway exhibits a lower h_{rms} (blueish color) compared to the west-east highway, which shows a higher h_{rms} (primarily cyan). Zooming in on the bridge of the west-east highway reveals a lower h_{rms} (blue) compared to the connecting roads at either end of the bridge (cyan). This suggests a sharp change in h_{rms}, potentially due to the use of

materials with lower surface roughness for bridge construction (see GE image in zoomed view).

VI. CONCLUSION

In this letter, a novel method for estimating road surface roughness using high-resolution spaceborne SAR datasets is proposed. The TS-X datasets used in this study exhibited good sensitivity to changes on road surfaces, indicating their potential for large-scale roughness estimation. The proposed semi-empirical model showed good agreement with both F-SAR results and GT data. However, the low SNR at the road areas in TS-X data, particularly for HH-polarized datasets, presents a significant challenge. For road surface roughness estimation, the best suitable data are VV polarized datasets acquired in ST-mode with steeper incidence angles of 30 to 35 degrees. This is because the ST mode can provide the highest spatial resolution, while the VV polarization and steeper incidence angles can ensure a higher SNR for road surfaces, thus providing better accuracy of the h_{rms} values. To remove incorrect values, it is necessary to apply upper σ^o and lower SNR thresholding on the h_{rms} images. Furthermore, when h_{rms} images from multiple datasets with different incidence angles are available, multi-dataset averaging can be applied to enhance the quality of the results. Road extraction and Google Earth visualization of the surface roughness images can help end users to interpret the results. A future high-resolution wide-swath SAR system (HRWS) with up to 1200 MHz bandwidth and better noise-equivalent sigma zero (NESZ) has the potential to improve road surface roughness estimation accuracy. Furthermore, systematic and repeated monitoring could also be used to detect road surface changes before and after winter, which could increase the robustness of road damage detection.

REFERENCES

[1] C. Y. Chan, B. Huang, X. Yan, and S. Richards, "Investigating effects of asphalt pavement conditions on traffic accidents in Tennessee based on the pavement management system (PMS)," *J Adv Transp*, vol. 44, no. 3, pp. 150–161, 2010.

[2] H. Liu, Z. Zhang, D. Guo, L. Peng, Z. Bao, and W. Han, "Research progress on characteristic technique of pavement micro-texture and testing technology of pavement skid resistance at home and abroad," in *2011 International Conference on Remote Sensing, Environment and Transportation Engineering*, 2011, pp. 4368–4372.

[3] A. Babu, S. V. Baumgartner, and G. Krieger, "Approaches for Road Surface Roughness Estimation Using Airborne Polarimetric SAR," *IEEE JSTARS*, vol. 15, pp. 3444–3462, 2022.

[4] E. Parliament *et al.*, *EU road surfaces: economic and safety impact of the lack of regular road maintenance*. Publications Office, 2014.

[5] M. I. Bani Baker, R. M. Abendeh, and M. A. Khasawneh, "Freeze and Thaw Effect on Asphalt Concrete Mixtures Modified with Natural Bentonite Clay," *Coatings*, vol. 12, no. 11, p. 1664, Nov. 2022.

[6] P. C. Dubois, J. van Zyl, and T. Engman, "Measuring soil moisture with imaging radars," *IEEE TGRS*, vol. 33, no. 4, pp. 915–926, Jul. 1995.

[7] Airbus Defence and Space, "TerraSAR-X Image Product Guide," Mar. 2015.

[8] I. Hajnsek, "Inversion of Surface Parameters Using Polarimetric SAR," Friedrich Schiller University Jena, 2001.

[9] M. Callens, N. E. C. Verhoest, and M. W. J. Davidson, "Parameterization of tillage-induced single-scale soil roughness from 4-m profiles," *IEEE TGRS*, vol. 44, no. 4, pp. 878–888, 2006.

[10] Airbus Defence and Space, "Radiometric Calibration of TerraSAR-X Data," Mar. 2014.

[11] A. Braun and L. Veci, "Sentinel-1 Toolbox SAR Basics Tutorial," 2020.